Nano Energy 92 (2022) 106681

Contents lists available at ScienceDirect

Nano Energy

journal homepage: www.elsevier.com/locate/nanoen

Over 18% ternary polymer solar cells enabled by a terpolymer as the third component

Wenhong Peng [a,b,d], Yuanbao Lin [c,*], Sang Young Jeong [e], Zewdneh Genene [b], Artiom Magomedov [f], Han Young Woo [e], Cailing Chen [h], Wandi Wahyudi [c], Qiang Tao [a], Jiyong Deng [a], Yu Han [h], Vytautas Getautis [f], Weiguo Zhu [d,*], Thomas D. Anthopoulos [c,*], Ergang Wang [b,g,**]

[a] Hunan Provincial Key Laboratory of Environmental Catalysis & Waste Re-cycling, School of Materials and Chemical Engineering, Hunan Institute of Engineering, Xiangtan 411104, China
[b] Department of Chemistry and Chemical Engineering, Chalmers University of Technology, Göteborg SE-412 96, Sweden
[c] King Abdullah University of Science and Technology (KAUST), KAUST Solar Center (KSC), Thuwal 23955, Saudi Arabia
[d] School of Materials Science and Engineering, Key Laboratory of Environmentally Friendly Polymer Materials of Jiangsu Province, Jiangsu Engineering Laboratory of Light-Electricity-Heat Energy-Converting Materials and Applications, Jiangsu Collaborative Innovation Center of Photovoltaic Science and Engineering, Changzhou University, Changzhou 213164, China
[e] Department of Chemistry, Korea University, Anam-ro 145, Seoul 02841, Republic of Korea
[f] Department of Organic Chemistry, Kaunas University of Technology, Kaunas LT-50254, Lithuania
[g] School of Materials Science and Engineering, Zhengzhou University, Zhengzhou 450001, China
[h] Advanced Membranes and Porous Materials Center, Physical Sciences and Engineering Division, King Abdullah University of Science and Technology, Thuwal 23955-6900, Saudi Arabia

ARTICLE INFO

Keywords:
Conjugated polymers
Compatible
High efficiency
Ternary organic solar cells
Terpolymer donor

ABSTRACT

"Ternary blending" and "random terpolymerization" strategies have both proven effective for enhancing the performance of organic solar cells (OSCs). However, reports on the combination of the two strategies remain rare. Here, a terpolymer PM6-Si30 was constructed by inserting chlorine and alkylsilyl-substituted benzodithiophene (BDT) unit (0.3 equivalent) into the state-of-the-art polymer PM6. The terpolymer exhibitsadeep highest-occupied-molecular-orbital energy and good miscibility with both PM6 and BTP-eC9 (C9) and enables its use as a third component into PM6:PM6-Si30:C9 bulk-heterojunction for OSCs. The resulting cells exhibit maximum power conversion efficiency (PCE) of 18.27%, which is higher than that obtained for the optimized control binary PM6:C9-based OSC (17.38%). The enhanced performance of the PM6:PM6-Si30:C9 cells is attributed to improved charge transport, favorable molecular arrangement, reduced energy loss and suppressed bimolecular recombination. The work demonstrates the potential of random terpolymer as a third component in OSCs and highlights a new strategy for the construction of a ternary system with improved photovoltaic performance.

1. Introduction

Organic solar cells (OSCs) have drawn great attention in the past decade as a potential clean energy source due to their unique advantages, such as light weight, flexibility, semitransparency and low-cost processing [1–5]. Typically, the active bulk heterojunction (BHJ) layer of OSCs is composed of one electron donor (D) and one electron acceptor (A) materials, leading to a combined absorption region and bandgap [6,7]. Ternary BHJs have been developed as a simple and reliable methodology to increase the power conversion efficiency (PCE) of single-junction OSCs by broadening the absorption spectrum, optimizing the blend morphology, balancing hole/electron mobilities, and reducing energy loss [8–13]. Recently, the PCE of ternary single-junction BHJ OSCs has increased rapidly to over 18% by

* Corresponding authors.
** Corresponding author at: Department of Chemistry and Chemical Engineering, Chalmers University of Technology, Göteborg SE-412 96, Sweden.
E-mail addresses: yuanbao.lin@kaust.edu.sa (Y. Lin), zhuwg18@126.com (W. Zhu), thomas.anthopoulos@kaust.edu.sa (T.D. Anthopoulos), ergang@chalmers.se (E. Wang).

https://doi.org/10.1016/j.nanoen.2021.106681
Received 17 August 2021; Received in revised form 9 October 2021; Accepted 29 October 2021
Available online 5 November 2021

employing conjugated polymers as donors, and Y-series small molecules as acceptors together with a third component such as small molecule D/A, fullerene-based acceptor, or a polymer donor [14–17].

One of the prerequisites for the third component in a successful ternary system is good compatibility with the other two host materials both in terms of chemical and electronic properties [18–23]. For example, two structurally similar Y6 derivations (Y6 and Y6-1O) were utilized as dual acceptors with D18-Cl donor, resulting in enhanced photon harvesting, minimized energy loss, and improved microstructure/morphology of the ternary BHJ [24]. As a result, high efficiency of 17.91% is obtained for the ternary OSC based on D18-Cl:Y6:Y6–1O due to the synchronously increased short-circuit current (J_{SC}), fill factor (FF) and open-circuit voltage (V_{OC}). The ternary strategy has proven to be effective for enhancing the performance in OSCs, however, most of the efficient ternary cases are based on two compatible acceptors (D:A1:A2) (See Table S1). Whereas two compatible donors (D1:D2:A) ternary systems are rarely studied [25–29] due to the lack of suitable materials.

Random terpolymers synthesized by introducing a third monomer into the backbone of host donor polymers (D1), provide a promising strategy for developing guest donor polymer (D2) as the third component for ternary (D1:D2:A) OSCs [30–32]. This type of terpolymers can be structurally similar to the host donor component, making them naturally compatible. The absorption spectra, energy levels, and aggregation behavior of the guest terpolymer can also be fine-tuned by rationally selecting the third monomer [33]. These advantageous characteristics make terpolymers ideal for use as the third component in ternary BHJs, which could ultimately help to boost the performance of ternary OSCs. However, this strategy has not been systematically explored in highly efficient OSCs.

Here, we employed PM6 as the host donor polymer and developed a new random terpolymer namely PM6-Si30 by introducing the chlorine (Cl) and alkylsilyl-substituted benzodithiophene (BDT) unit as the third monomer to replace 0.3 equivalent of the fluorine (F) and alkyl-substituted BDT unit in PM6 (Fig. 1a). The terpolymer PM6-Si30 exhibits a lower highest occupied molecular orbital (HOMO) level with slightly blue-shifted absorption as compared to PM6. Therefore, the terpolymer PM6-Si30 can potentially be utilized as the third component in a binary system, such as PM6:BTP-eC9 (C9), due to the structural similarity with the PM6, good compatibility and miscibilty with both the PM6 and C9 as well as the favorable energetics. Indeed, we found that the incorporation of 15 wt% of PM6-Si30 (D2) into PM6:C9 (D1:A) binary device, yield devices with simultaneously improved V_{OC} (0.87 V), J_{SC} (26.90 mA cm^{-2}) and FF (78.04%), resulting in a maximum PCE of 18.27%. To our knowledge, this is among the highest values for ternary OSCs in a D1:D2:A system reported to date (Table S1, Supporting Information). The enhanced performance of the ternary OSCs based on PM6:PM6-Si30:C9 is ascribed to the propitious phase separation, enhanced crystallinity, reduced recombination loss and long carrier lifetime in the active layer. Our work highlights the potential of random terpolymer derived from the host donor polymer as a highly effective strategy for improving the performance of ternary OSCs.

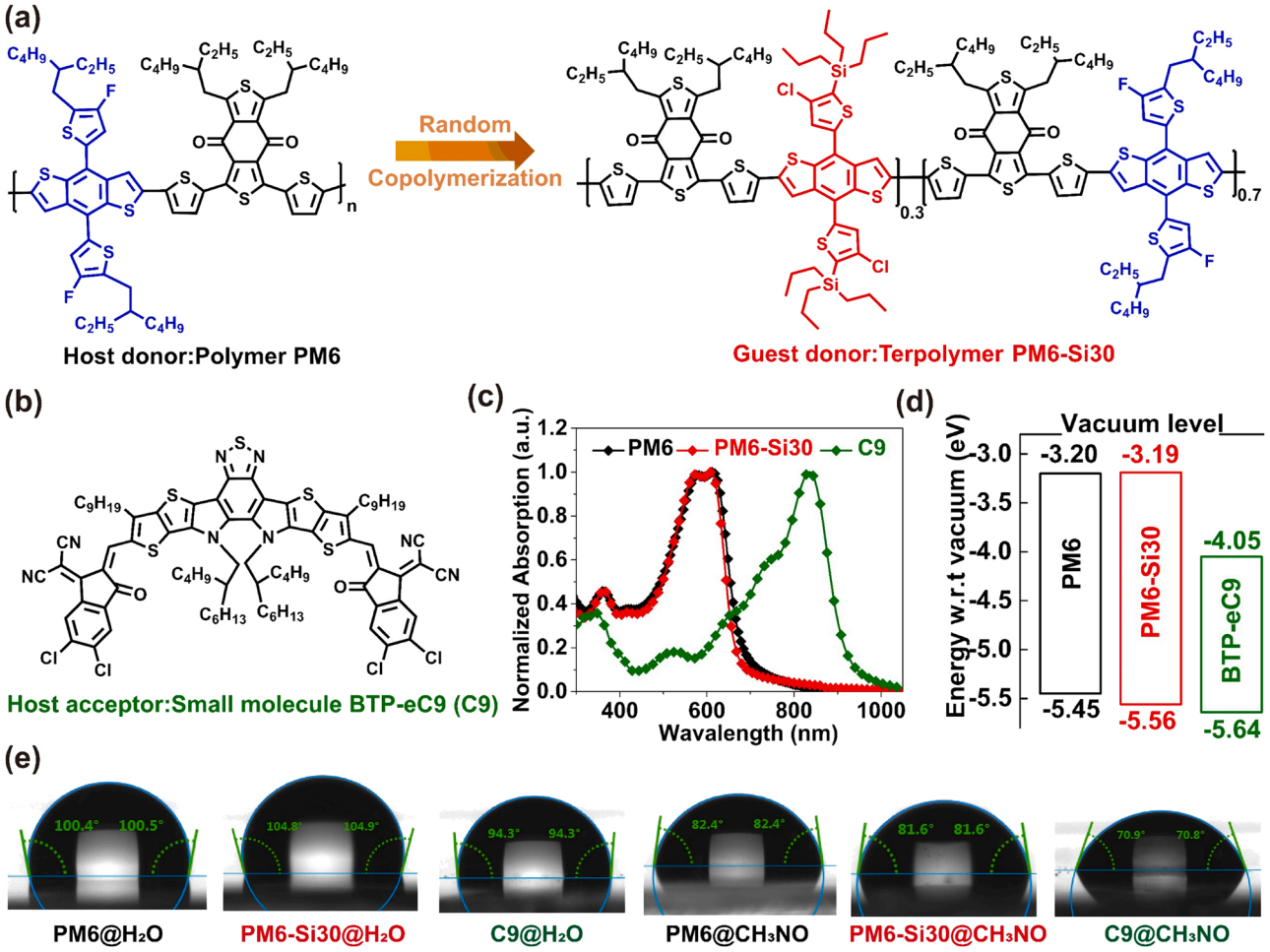

Fig. 1. (a) Chemical structures of PM6 and PM6-Si30. (b) Chemical structure of BTP-eC9 (C9); (c) Normalized UV−vis absorption spectra of PM6, PM6-Si30, and C9 in film; (d) Energy levels of PM6, PM6-Si30, and C9; (e) The contact angle images of PM6, PM6-Si30 and C9 films performed by using deionized water (H_2O) and formamide (CH_3NO) as wetting liquids.

2. Results and discussion

Fig. 1a and b show the molecular structures of the active materials used in this study, i.e. PM6, PM6-Si30, and C9. The terpolymer PM6-Si30 was prepared by Stille coupling reaction of monomer **1** with **2** and **3**, using $Pd(PPh_3)_4$ as a catalyst and the detailed synthetic procedure of terpolymer PM6-Si30 is shown in the experimental section of the Supporting Information (Scheme S1). The ^1H, ^{13}C NMR spectrum of the terpolymer PM6-Si30 are presented in Fig. S1. The new terpolymer PM6-Si30 shows good solubility in commonly used organic solvents such as chloroform, chlorobenzene, and *o*-dichlorobenzene. The number average molecular weight (M_n) was 23.3 kDa with polydispersity (PDI) of 3.41, measured by gel permeation chromatography (GPC) using 1,2,4-trichlorobenzene as the eluent and linear polystyrene as the reference at 150 ℃ (Fig. S2,Table S2). The weak electron-withdrawing Cl atoms and alkylsilyl side-chains on the BDT unit of the third momomer is beneficial to adjusting the key properties including absorption spectra, energy levels, and surface energy of the new terpolymer PM6-Si30 [34–37]. The UV–vis absorption spectra of PM6, PM6-Si30, and C9 neat films were measured and shown in Fig. 1c. The absorption spectrum of the PM6-Si30 film is slightly blue-shifted (613–608 nm) with the absorption edge located at around 670 nm as compared to PM6. The optical bandgap estimated from the onsets of the absorption of the solid films were 1.85 and 1.82 eV for PM6-Si30 and PM6, respectively. Although the terpolymer PM6-Si30 exhibits very analogous absorption profiles with that of the host polymer PM6, its absorption coefficient is higher between 300 and 650 nm (Fig. S3). Such difference could potentially yield improved photon harvesting and hence cells with higher PCE.

Cyclic voltammetry (CV) measurements were performed to determine the HOMO and the lowest unoccupied molecular orbital (LUMO) energy levels of the two polymers (Fig. S4). The energy levels of these materials are shown in Fig. 1d where the HOMO/LUMO levels of PM6 and PM6-Si30 are −5.45/−3.20 eV and −5.56/−3.19 eV, respectively (Table S3). When compared with the host donor PM6, the PM6-Si30 shows a lower HOMO level, which may benefit the V_{OC} in ternary OSCs [27]. The difference in the HOMO of the terpolymer PM6-Si30 was confirmed by photoelectron spectroscopy in air (PESA) measurements (Fig. S5), where the HOMO of PM6-Si30 appears at around −5.27 eV, which is slightly deeper than that of PM6 (around −5.18 eV). Moreover, the HOMO/LUMO levels of PM6:PM6-Si30 blend with optimal blending ratios (0.85:0.15) were measured by CV and PESA techniques (Fig. S4 and Fig. S5d). The optimal PM6:PM6-Si30 blend showed the same frontier orbital (HOMO and LUMO) energies based on the average composition of these two components, which indicates the formation of an alloy [38,39]. Therefore, the V_{OC} in the ternary OSCs should vary gradually as the composition of the two donors changes.

The terpolymer PM6-Si30 consists of a 30% ClSi-BDT unit which has a very similar chemical structure with PM6, making the two polymers highly compatible. To further confirm this hypothesis, we measured the contact angles of the neat films of PM6, PM6-Si30, C9, and three blend films using deionized water (H_2O) and formamide (CH_3NO) as wetting liquids (Fig. 1e and Fig. S6). The surface energy value (γ) for each system was inferred using the Owens, Wendt, Rabel, and Kaelble (OWRK) equation [40] yielding 20.3, 24.4, and 29.5 mN m^{-1}, for PM6, PM6-Si30 and C9, as well as 22.7, 25.6, and 26.7 mN m^{-1} for PM6:C9, PM6:PM6-Si30:C9, and PM6-Si30:C9, respectively (Table S4-S5). Therefore, good compatibility between these two donor polymers can be expected as indicated by their similar surface energy. The miscibility between the three materials in blends was further estimated by the Flory-Huggins interaction parameter χ using the equation $\chi_{A-B} \propto \left(\sqrt{\gamma_A} - \sqrt{\gamma_B}\right)^2$ [41], where γ_A and γ_B are the surface energy values of component A and B calculated from the contact angle measurements, respectively. The χ parameter was calculated as 0.86, 0.24, 0.19, for PM6:C9, PM6-Si30:C9, PM6:PM6-Si30, respectively. The χ values for PM6-Si30:C9 and PM6:PM6-Si30 are much lower than that of PM6:C9, suggesting the terpolymer of PM6-Si30 is compatible with both PM6 and C9. Based on these measurements, one may argue that the solid film containing the two donor polymers resembles an alloyed state in the ternary blend which still facilitates the formation of proper phase separation between donor and acceptor components [42,43].

The photovoltaic properties of the binary (PM6:C9 and PM6-Si30:C9) and ternary (PM6:PM6-Si30:C9) blends were investigated by integrating them in cells consisting of indium tin oxide (ITO)/[2-(3,6-dibromo-*9H*-carbazol-9-yl)ethyl]phosphonic acid (Br-2PACz)/active layer / poly[(9,9-bis(3′-(N,N-dimethylamino)propyl)-2,7-fluorene)-alt-5,5′-bis(2,2′-thiophene)-2,6-naphthalene-1,4,5,8-tetracaboxylic-N,N′-di(2-ethylhexyl)imide] (PNDIT-F3N)/Ag (Fig. 2a). The weight ratio of the donor(s) to acceptor was kept constant at 1:1.2 (wt./wt.). The current density-voltage (*J-V*) of the ternary BHJ cells with different PM6-Si30 content are presented in Fig. S7 and Table S6. Fig. S8 shows the efficiency histograms of the optimal binary and ternary devices. The *J-V* curves of the optimized binary and ternary OSCs are displayed in Fig. 2b, and the corresponding photovoltaic parameters are summarized in Table 1. A maximum PCE of 17.38% was obtained for the binary PM6:C9-based OSCs with J_{SC} of 26.58 mA cm^{-2}, V_{OC} of 0.852 V and FF of 76.73%. On the other hand, the binary PM6-Si30:C9-based OSCs exhibited a relatively low PCE of 14.32% primarily due to the low J_{SC} of 24.69 mA cm^{-2} and FF of 65.37%. Despite the lower performance, the cells produce a higher V_{OC} (0.887 V) as compared to PM6:C9-based devices (0.852 V) thanks to the deeper HOMO of PM6-Si30 (−5.56 eV vs. −5.45 eV). Thus, the V_{OC} of ternary OSCs increases gradually with increasing PM6-Si30 content, indicating the prevailing role of the reduced HOMO in the formed PM6:PM6-Si30 alloy [44–46].

We were able to boost the PCE of ternary OSCs to 18.27% by incorporating 15 wt% PM6-Si30 in the blend (Table 1). This significant enhancement is the result of the simultaneously improved J_{SC} (26.90 mA cm^{-2}), FF (78.04%) and V_{OC} (0.870 V). As shown in Fig. 2c PM6:PM6-Si30:C9-based OSCs exhibit higher EQE as compared to binary PM6:C9-based devices, primarily between 450 and 600 nm (ΔEQE in Fig. 2c). The latter characteristic is, at least partially, attributed to the higher absorption coefficient of the terpolymer PM6-Si30 (Fig. S3), which in turn results in higher photocurrent for ternary devices as compared to binary cells (26.90 mA cm^{-2} vs. 26.58 mA cm^{-2}). In addition, the current density values integrated from the EQE spectra are in good agreement with the J_{SC} values and within a 3% mismatch, indicating the reliability of the measured photovoltaic data. Fig. S9 shows the parasitic absorption and internal quantum efficiency (IQE) spectra of PM6:C9 and PM6:PM6-Si30:C9-based OSCs. The two devices show similar absorption spectra, but higher IQE_{AVE} values for PM6:PM6-Si30:C9 device (88.6%) as compared with PM6:C9 device (87.4%). These findings suggest that the higher EQE values are primarily attributed to slightly enhanced charge generation and extraction in the optimized ternary devices.

The dependence of V_{OC} and J_{SC} on the light intensity (P_{light}) were measured to study the recombination mechanism for the binary and ternary devices (Fig. 2d and Fig. S10). Here, a slope of $1 \times kT/q$ is expected for bimolecular recombination dominated devices in the plot of V_{OC} versus the natural logarithm of the light intensity, where k is Boltzmann constant, q is the elementary charge, and T is temperature [47]. PM6:C9 cell exhibits a slope of 1.12 kT/q, suggesting the existence of recombination due to traps. This trap-assisted recombination is drastically reduced upon the addition of 15 wt% PM6-Si30 (slope 1.04 kT/q), in agreement with the higher FF and better performance obtained in the ternary device (Fig. 2d).

On the other hand, the dependence of J_{SC} on P_{light} can be described as $J_{SC} \propto P_{light}^{\alpha}$ [48,49], where α refers to the exponential factor, which can be calculated from the slope of the $\log(J_{SC})$-$\log(P_{light})$ [50,51]. As illustrated in Fig. S10, the PM6:PM6-Si30:C9 ternary device yields a higher value of 0.98, while the two binary devices based on PM6:C9 and

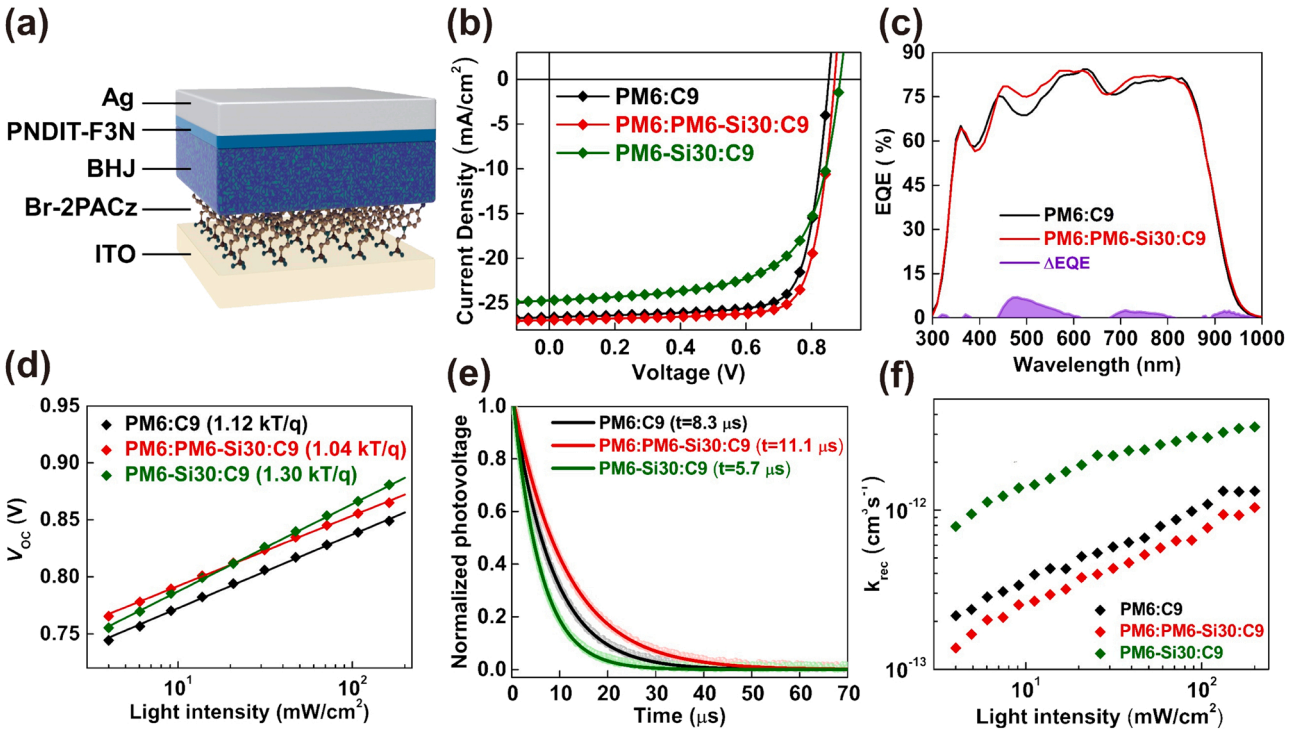

Fig. 2. (a) The schematic architecture of OSC device; (b) *J-V* characteristics and (c) EQE curves for optimized devices based on PM6:C9, PM6:PM6-Si30:C9, as well as their difference ΔEQE; (d) Light intensity dependence of V_{oc} for the optimized binary and ternary OSC devices; (e) TPV spectra, and (f) Light intensity dependence of bimolecular recombination rate constant (k_{rec}) for the optimized binary and ternary OSC devices.

Table 1
Photovoltaic parameters of the binary and ternary OSCs, measured under the illumination of AM 1.5 G at 100 mW/cm^2.

PM6:PM6-Si30:C9	V_{OC} [V]	J_{SC} [mA cm^{-2}]	*Calc.* J_{SC}[a] [mA cm^{-2}]	FF [%]	PCE_{max} (PCE_{avg})[b] [%]
1:0:1.2	0.852	26.58	25.75	76.73	17.38 (17.0 ± 0.2)
0.85:0.15:1.2	0.870	26.90	26.22	78.04	18.27 (17.9 ± 0.3)
0:1:1.2	0.887	24.69	23.90	65.37	14.32 (14.1 ± 0.1)

[a] Calculated J_{SC} from EQE measurement.
[b] The average PCE values with standard deviations were obtained from 15 different cells.

PM6-Si30:C9 exhibit lower values of 0.96 and 0.94, respectively. The value of α closer to 1 for the ternary device suggests that the incorporation of PM6-Si30 reduces bimolecular recombination in the cell, thereby leading to the higher J_{SC} and FF values.

We also performed transient photovoltage (TPV) measurements to examine the lifetime of photocarriers in the optimized binary and ternary OSCs. As shown in Fig. 2e, the recombination time of photocarriers (τ_{rec}) for the ternary device (τ_{rec}= 11.1 μs) is longer than the values obtained for two binary devices (τ_{rec}= 8.3, 5.7 μs), implying suppression of charge recombination. Fig. 2f displays the light intensity dependence of bimolecular recombination rate constant (k_{rec}) for the binary and ternary OSCs. The value of k_{rec} for the ternary PM6:PM6-Si30:C9 device is lower than that of the two binary devices at all light intensities investigated. The above results verify that the improved photovoltaic performance in the ternary OSCs originates from the lower recombination losses [52].

Space charge limited current (SCLC) measurements were performed to evaluate the hole and electron mobilities (μ_h and μ_e) of the neat films, and binary and ternary blends. Representative curves are shown in Fig. S11 while the extracted data are summarized in Tables S7-S8. The pristine PM6-Si30 film shows a slightly higher μ_h of 2.5 × 10^{-4} cm^2 V^{-1} s^{-1} as compared to that of PM6 1.6 × 10^{-4} cm^2 V^{-1} s^{-1}. Interestingly, blend layers of PM6-Si30:C9 exhibits a higher μ_e (3.0 ×10^{-4} cm^2 V^{-1} s^{-1}) than the PM6:C9 blend (1.7 ×10^{-4} cm^2 V^{-1} s^{-1}) with the μ_h values remaining the same and comparable (1.3 ×10^{-4} cm^2 V^{-1} s^{-1} vs. 1.4 ×10^{-4} cm^2 V^{-1} s^{-1}). The unbalanced μ_e/μ_h of 2.31 is the most likely reason for the low FF measured in PM6-Si30:C9-based devices (Table 1). Interestingly, the addition of 15 wt% PM6-Si30 in the PM6:C9 blend (PM6:PM6-Si30:C9), increases both the μ_h and μ_e yielding values of 2.2 × 10^{-4} cm^2 V^{-1} s^{-1} and 2.4 × 10^{-4} cm^2 V^{-1} s^{-1}, respectively, that are approximately 1.6 times and 1.4 times higher than the μ_h and μ_e of the binary PM6:C9 blend. The improved ambipolar charge transport is possibly the result of a more favorable active layer morphology due to enhanced molecular packing in the ternary blend film (discussed below). This improvement leads to a more balanced charge transport with a μ_h/μ_e value of 0.96 for the ternary PM6:PM6-Si30:C9 film as compared to the binary PM6:C9 film (1.13), ultimately contributing to the slightly higher FF (78.04% vs. 76.73%).

To examine the surface morphology of the neat, binary and ternary layers, we used atomic force microscopy (AFM) in non-contact tapping mode (Fig. 3). When compared to the two donor polymers, the small molecule acceptor C9 appears to aggregate yielding relatively rough layers with a high root-mean-square (RMS) surface roughness of 11.7 nm. The surface morphologies of PM6 and the terpolymer PM6-Si30, on the other hand, are similar with the latter exhibiting slightly smaller nanofiber-like features ultimately resulting in a lower RMS value of 0.73 nm as compared to 1.12 nm for PM6. The smaller-size nanofiber-like morphology of PM6-Si30 is expected to lead to improved mixing with both PM6 and C9, potentially resulting in more favorable phase separation between the donor and acceptor components. This hypothesis is supported by the reduction of the RMS values from 1.48 nm for the binary PM6:C9, to 1.25 nm for the ternary PM6:PM6-Si30:C9 blend upon addition of 15%wt PM6-Si30. Indeed, these results suggest good miscibility between PM6-Si30, PM6 and C9 components, which most likely also underpins the improved charge transport and ultimately

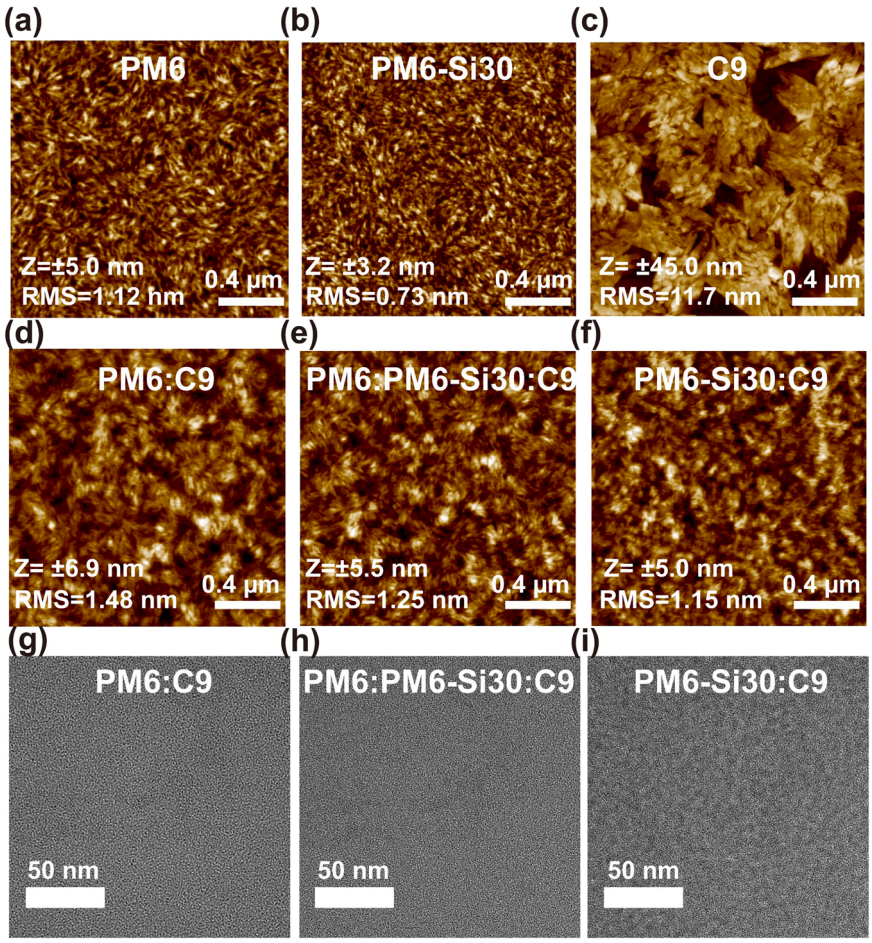

Fig. 3. Tapping mode AFM topography images of (a,b,c) PM6, PM6-Si30, C9 neat films, and (d, e, f) PM6:C9, PM6:PM6-Si30:C9, PM6-Si30:C9 blend films; The size of the AFM image is 2 μm × 2 μm (The size of C9 is 10 μm × 10 μm). TEMs images of (g, h, i) PM6:C9, PM6:PM6-Si30:C9, PM6-Si30:C9 blend films.

higher photovoltaic performance observed in agreement with previous results [53,54]. Further insight into the microstructure of the different blends were obtained from transmission electron microscopy (TEM) measurements (Fig. 3g–i). Of particular interest is the TEM image of the PM6-Si30:C9 blend which reveals a clear phase separation manifested as white and dark domains. When the terpolymer PM6-Si30 is added as a third component in the PM6:C9 blend, the ensuing ternary PM6:PM6-Si30:C9 layer exhibits a very similar morphology (i.e. highly homogeneous) to the binary PM6:C9 blend film. Details of the different microstructures will be discussed later.

The impact of PM6-Si30 on the crystallinity and molecular packing of the BHJ was also characterized using grazing-incidence wide-angle X-ray scattering (GIWAXS) measurements. As shown in Fig. 4 and Tables S9-S10, pristine PM6 film exhibits clear (100) and (010) diffraction peaks in both the in-plane (IP) and out-of-plane (OOP) directions at $q_{xy} = 0.29$ Å^{-1} ($d = 22.44$ Å) and $q_z = 1.67$ Å^{-1} ($d = 3.76$ Å), respectively. The diffraction pattern of PM6-Si30 changes subtly due to the addition of the 30% ClSi-BDT unit, yielding a loosen cofacial π-π staking with an increased (010) *d*-spacing (3.83 Å) in the OOP direction and enhanced lamellar interdigitation ($d = 21.37$ Å) in the IP direction. The latter feature, also seen in other systems [55], may be responsible for the higher hole mobility measured in pristine PM6-Si30 layers. On the other hand, the C9 film exhibits a preferred face-on orientation with a (100) lamellar peak at $q_{xy} = 0.39$ Å^{-1} ($d = 16.11$ Å) and a (010) peak at $q_z = 1.70$ Å^{-1} ($d = 3.70$ Å). The PM6:C9 blend layer retains a dominant face-on orientation with two (100) lamellar peaks at $q_{xy} = 0.29$ and 0.39 Å^{-1} ($d = 21.67$, and 16.11 Å), and a (010) peak at $q_z = 1.71$ Å^{-1} ($d = 3.67$ Å). Meanwhile, the ternary PM6:PM6-Si30:C9 (0.85:0.15:1.2) blend exhibits almost the same molecular orientation, but based on the OOP (010) peak, the *d*-spacing value decreases slightly from 3.70 to 3.67 Å. The latter leads to a notable increase in the crystalline coherence length (CCL) value from 25.13 Å (PM6:C9 binary blend) to 28.56 Å (PM6:PM6-Si30:C9 ternary blend), suggesting an enhanced *π*-*π* stacking. This enhancement is most likely responsible for a slightly improved charge transport upon the addition of 15 wt% PM6-Si30.

Next, the impact of the introduced guest donor terpolymer on energy losses (E_{loss}) in PM6:C9 devices, was studied. We first measured the optical bandgaps (E_g) of PM6:C9 and PM6:PM6-Si30:C9 blends, with both yielding the same value of ~1.38 eV (Fig. S12). As summarized in Table 2, the incorporation of PM6-Si30 has a minor impact on E_{loss} (0.51 eV) as compared to PM6:C9 (0.53 eV). This implies that the addition of PM6-Si30 can potentially improve the V_{OC} in ternary cells with no adverse effects. We also measured the highly sensitive EQE (sEQE) and electroluminescence (EL) spectra of the cells (Fig. 5a-b). The different losses processes where then analyzed to obtain the total E_{loss} using [56,57]: $E_{loss} = \Delta E_1 + \Delta E_2 + \Delta E_3$, where ΔE_1 originates from radiative recombination loss above the band-gap, ΔE_2 comes from radiative recombination energy loss and ΔE_3 is attributed to non-radiative recombination energy loss. The detailed calculations of the energy loss components (i.e. ΔE_1, ΔE_2, ΔE_3) can be found in Supplemental Information. For any types of solar cells, the ΔE_1 is unavoidable and is typically ≥ 0.25 V. We found that the two types of devices show the same ΔE_1 of ≈ 0.27 eV, whereas the ΔE_2 and ΔE_3 values are relatively low in the ternary devices as compared with the binary devices. As depicted in Fig. 5c, the optimized PM6:PM6-Si30:C9 ternary device exhibits a higher EQE_{EL} (4.2×10^{-4}) than the binary

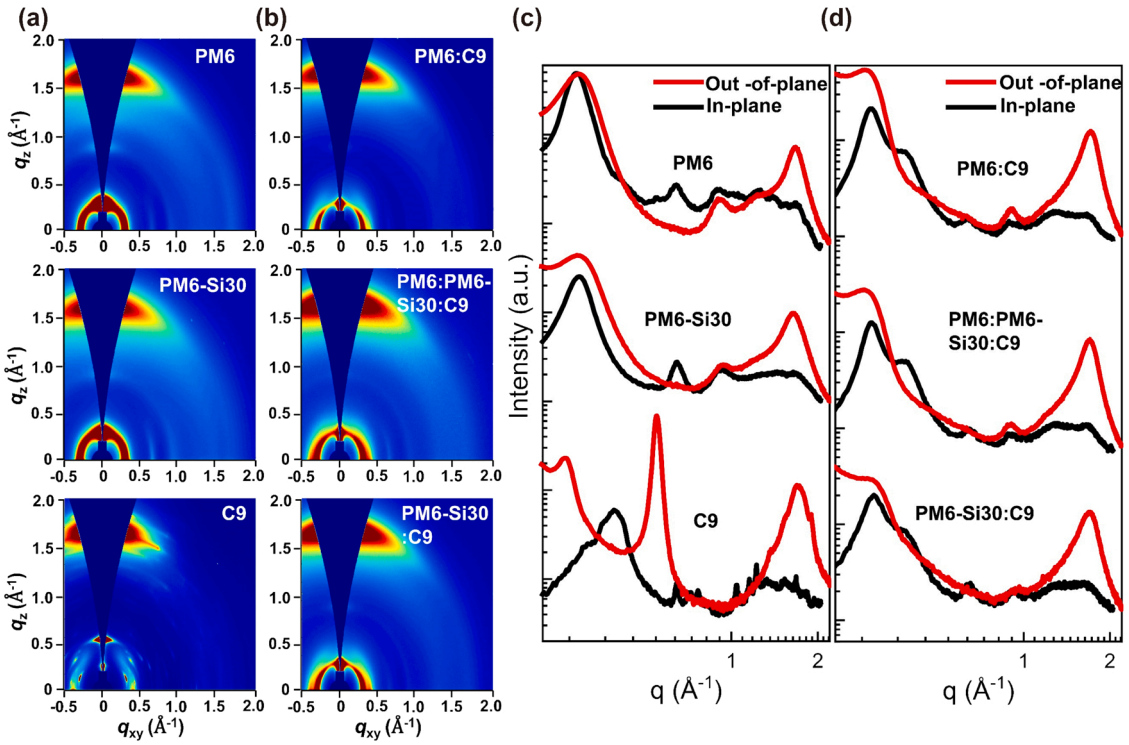

Fig. 4. (a) GIWAXS patterns and (c) scattering profiles of in-plane and out-of-plane for neat PM6, PM6-Si30 and C9; (b) GIWAXS patterns and (d) scattering profiles of in-plane and out-of-plane for PM6:C9, PM6:PM6-Si30:C9, and PM6-Si30:C9 blend films.

Table 2
Detailed energy losses of the optimized PM6:C9-based binary and PM6:PM6-Si30:C9-based ternary OSCs.

Devices	E_g[a] (eV)	E_{loss} (eV)	$V_{OC,\ SQ}$[b] (eV)	E_{CT} (eV)	EQE_{EL}	ΔE_1 (eV)	ΔE_2 (eV)	ΔE_3[c](eV)
PM6:C9	1.38	0.53	1.11	1.35	2.5×10^{-4}	0.27	0.05	0.22
PM6:PM6-Si30:C9	1.38	0.51	1.12	1.36	4.2×10^{-4}	0.27	0.04	0.20

[a] E_g is the optical bandgap of the film calculated on the basis of the intersections between the normalized absorption and EL spectra of films.
[b] $V_{OC,\ SQ}$ is the maximum V_{oc} by the SQ limit.
[c] ΔE_3 is calculated from the EQE_{EL} measured by a silicon detector.

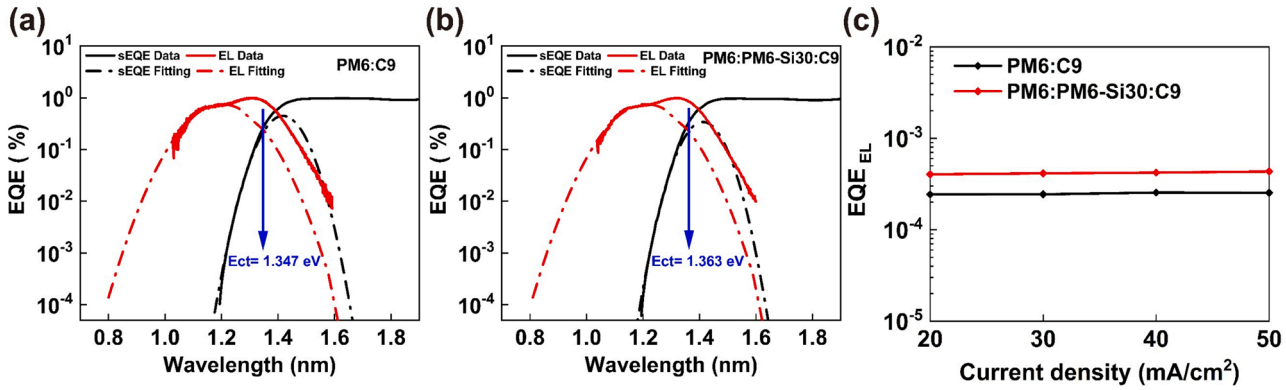

Fig. 5. The sEQE and EL spectra of OSCs devices based on (a) PM6:C9 and (b) PM6:PM6-Si30:C9 blends; (c) EL quantum efficiencies of the optimized PM6:C9-based binary and PM6:PM6-Si30:C9-based ternary OSCs.

PM6:C9 cell (2.5×10^{-4}), thus leading to the reduced non-radiative losses. These results indicate that addition of PM6-Si30 as the third component in OSCs, helps on one hand to reduce losses associated with nonradiative recombination, and on the other increase the cell's V_{OC}.

Finally, we note the several previous studies highlighted the positive impact of a third component on OSCs' stability and performance [58–60]. To test whether the terpolymer PM6-Si30 can work as a rational morphology stabilizer, we performed stability test on both PM6:C9 and PM6:PM6-Si30:C9 devices. Optimized cells were stored inside a glove box and thermally annealed for 95 h at 100 ℃ after which were fully tested (Fig. S13a). Evidently, cells based on the ternary PM6:PM6-Si30:C9 (0.85:0.15:1.2) retain 55% of the initial PCE, whereas cells based on PM6:C9 (1:1.2) retained only 47%, clearly highlighting the beneficial role of the terpolymer. Moreover, we tested the PM6:C9

and PM6:PM6-Si30:C9 cells (un-encapsulated inside the glovebox) under continuous illumination (100 mW/cm^2) for an initial period of 80 h (Fig. S13b). The ternary PM6:PM6-Si30:C9 device exhibits relatively high photostability, retaining 20% of its initial performance after 80 h. Meanwhile, the performance of PM6:C9 cell dropped to 13% of its initial value. These results strongly suggest that addition of the terpolymer PM6-Si30 as the third component in PM6:C9 blend improves both the photovoltaic properties and thermal/photo-stability of the ensuing OSCs. Most importantly, the work highlights an interesting strategy for the development of a gamut of new polymeric materials for application in OSCs.

3. Conclusions

In summary, we have designed and synthesized a random terpolymer, namely PM6-Si30, and used it as the guest donor in ternary PM6:PM6-Si30:C9 organic solar cells. Adding 15 wt% PM6-Si30 into the PM6:C9 blend resulted in BHJs with nano-fiber like surface morphologies and enhanced π-π stacking. These changes were found to balance as well as increase the hole and electron mobilities while simultaneously suppressing the trap-assisted and bimolecular recombination rates and thereby improving both the FF and J_{SC}. Furthermore, the presence of the PM6-Si30 with a deeper HOMO level in the BHJ helped to reduce the E_{loss}, leading to solar cells with higher V_{OC}. As a result of these synergistic effects, ternary OSCs with a higher PCE of 18.27% were obtained as compared to 17.38% of the control binary cells. Importantly, the addition of PM6-Si30 into the binary PM6:C9 blend not only improves the photovoltaic performance of the cells but also their thermal and photo-stability characteristics, making the approach particularly attractive for applications in OSCs.. Our work demonstrates how the use of terpolymers with structural similarities to the host donor polymer can be exploited to boost the performance of ternary OSCs, paving the way to future developments in new materials and advanced material formulations.

CRediT authorship contribution statement

Wenhong Peng: Synthesis, Formal analysis, Writing – original draft. **Yuanbao Lin:** Device preparation and characterization, Writing – review & editing. **Sang Young Jeong & Han Young Woo:** GIWAXS measurement and analysis, Data curation. **Zewdneh Genene:** CV measurement and analysis, Writing – review & editing. **Artiom Magomedov & Vytautas Getautis:** Synthesis, Conceptualization. **Cailing Chen & Yu Han:** TEM measurement; **Qiang Tao & Jiyong Deng:** Visualization, Investigation. **Wandi Wahyudi:** NMR measurement; **Weiguo Zhu:** Writing – review & editing. **Thomas D. Anthopoulos:** Writing – review & editing, Funding acquisition, Supervision. **Ergang Wang:** Writing – review & editing, Supervision, Project administration.

Declaration of Competing Interest

The authors declare that they have no known competing financial interests or personal relationships that could have appeared to influence the work reported in this paper.

Acknowledgements

We thank the Swedish Research Council (2016-06146, 2019-04683), the Swedish Research Council Formas and the Knut and Alice Wallenberg Foundation (2017.0186, 2016.0059) for financial support. This work is also supported by the National Natural Science Foundation of China (51673031, 51573154), the Major Program of the Natural Science Research of Jiangsu Higher Education Institutions (18KJA480001), the Top-notch Academic Programs Project (TAPP) for Polymeric Materials Science and Engineering & the Priority Academic Program Development (PAPD) of Jiangsu Higher Education Institutions, Jiangsu Provincial Talents Project of High-Level Innovation and Entrepreneurship, and the Foundation of State Key Laboratory of Polymer Materials Engineering (sklpme2017-2-04). W. P. thanks the support by China Scholarship Council, and Y. L., and T. D. A. by the King Abdullah University of Science and Technology (KAUST) Office of Sponsored Research (OSR) under Award No: OSR-2018-CARF/CCF-3079, and No: OSR-2019-CRG8-4095.3. H.Y.W acknowledges the financial support from the National Research Foundation (NRF) of Korea (2019R1A6A1A11044070).

Appendix A. Supporting information

Supplementary data associated with this article can be found in the online version at doi:10.1016/j.nanoen.2021.106681.

References

[1] J. Wang, X. Zhan, Fused-ring electron acceptors for photovoltaics and beyond, Acc. Chem. Res. 54 (2021) 132–143.
[2] M. Polman, E.C. Knight, B. Garnett, W.C. Ehrler Sinke, Photovoltaic materials: present efficiencies and future challenges, Science 352 (2016), aad4424.
[3] Q. Fan, U.A. Mendez-Romero, X. Guo, E. Wang, M. Zhang, Y. Li, Fluorinated photovoltaic materials for high-performance organic solar cells, Chem. Asian J. 14 (2019) 3085–3095.
[4] J. Chen, Y. Chen, L.-W. Feng, C. Gu, G. Li, N. Su, G. Wang, S.M. Swick, W. Huang, X. Guo, A. Facchetti, T.J. Marks, Hole (donor) and electron (acceptor) transporting organic semiconductors for bulk-heterojunction solar cells, EnergyChem 2 (2020), 100042.
[5] Q. Fan, H. Fu, Q. Wu, Z. Wu, F. Lin, Z. Zhu, J. Min, H.Y. Wu, A.K.-Y. Jen, Multi-selenophene-containing narrow bandgap polymer acceptors for all-polymer solar cells with over 15% efficiency and high reproducibility, Angew. Chem. Int. Ed. 60 (2021) 15935–15943.
[6] Y. Huang, E.J. Kramer, A.J. Heeger, G.C. Bazan, Bulk heterojunction solar cells: morphology and performance relationships, Chem. Rev. 114 (2014) 7006–7043.
[7] C.-H. Duan, F. Huang, Y. Cao, N.S. Sariciftci, Y. Li, G.C. Bazan, X. Gong, Organic Materials and Chemistry for Bulk Heterojunction Solar Cells, Wiley-VCH Verlag GmbH & Co. KGaA, 2012.
[8] X. Liu, Y. Yan, Y. Yao, Z. Liang, Ternary blend strategy for achieving high-efficiency organic solar cells with nonfullerene acceptors involved, Adv. Funct. Mater. 28 (2018), 1802004.
[9] P. Bi, S. Zhang, Z. Chen, Y. Xu, Y. Cui, T. Zhang, J. Ren, J. Qin, L. Hong, X. Hao, J. Hou, Reduced non-radiative charge recombination enables organic photovoltaic cell approaching 19% efficiency, Joule 5 (2021) 2408–2419.
[10] L. Chang, M. Sheng, L. Duan, A. Uddin, Ternary organic solar cells based on non-fullerene acceptors: a review, Org. Electron. 90 (2021), 106063.
[11] P. Bi, X. Hao, Versatile ternary approach for novel organic solar cells: a review, Sol. RRL 3 (2019), 1800263.
[12] Y. Lin, M.I. Nugraha, Y. Firdaus, A.D. Scaccabarozzi, F. Anies, A.-H. Emwas, E. Yengel, X. Zheng, J. Liu, W. Wahyudi, E. Yarali, H. Faber, O.M. Bakr, L. Tsetseris, M. Heeney, T.D. Anthopoulos, A simple n-dopant derived from diquat boosts the efficiency of organic solar cells to 18.3%, ACS Energy Lett. 5 (2020) 3663–3671.
[13] W. Peng, Y. Lin, S.Y. Jeong, Y. Firdaus, Z. Genene, A. Nikitaras, L. Tsetseris, H. Y. Woo, W. Zhu, T.D. Anthopoulos, E. Wang, Using two compatible donor polymers boosts the efficiency of ternary organic solar cells to 17.7%, Chem. Mater. 33 (2021) 7254–7262.
[14] Y. Lin, A. Magomedov, Y. Firdaus, D. Kaltsas, A. El-Labban, H. Faber, D. R. Naphade, E. Yengel, X. Zheng, E. Yarali, N. Chaturvedi, K. Loganathan, D. Gkeka, S.H. AlShammari, O.M. Bakr, F. Laquai, L. Tsetseris, V. Getautis, T. D. Anthopoulos, 18.4% Organic solar cells using a high ionization energy self-assembled monolayer as hole-extraction interlayer, ChemSusChem 14 (2021) 1–11.
[15] Y. Lin, B. Adilbekova, Y. Firdaus, E. Yengel, H. Faber, M. Sajjad, X. Zheng, E. Yarali, A. Seitkhan, O.M. Bakr, A. El-Labban, U. Schwingenschlogl, V. Tung, I. McCulloch, F. Laquai, T.D. Anthopoulos, 17% Efficient organic solar cells based on liquid exfoliated WS2 as a replacement for PEDOT:PSS, Adv. Mater. 31 (2019), 1902965.
[16] K. Jin, Z. Xiao, L. Ding, 18.69% PCE from organic solar cells, J. Semicond. 42 (2021), 060502.
[17] X. Chen, D. Wang, Z. Wang, Y. Li, H. Zhu, X. Lu, W. Chen, H. Qiu, Q. Zhang, 18.02% Efficiency ternary organic solar cells with a small-molecular donor third component, Chem. Eng. J. 424 (2021), 130397.
[18] K. Weng, C. Li, P. Bi, H.S. Ryu, Y. Guo, X. Hao, D. Zhao, W. Li, H.Y. Woo, Y. Sun, Ternary organic solar cells based on two compatible PDI-based acceptors with an enhanced power conversion efficiency, J. Mater. Chem. A 7 (2019) 3552–3557.
[19] X. Wang, Q. Sun, J. Gao, X. Ma, J.H. Son, S.Y. Jeong, Z. Hu, L. Niu, H.Y. Woo, J. Zhang, F. Zhang, Ternary organic photovoltaic cells exhibiting 17.59% efficiency with two compatible Y6 derivations as acceptor, Sol. RRL 5 (2021), 2100007.
[20] Z. Su, Z. Zhang, G. Xie, Y. Zhang, X. Zhang, W. Zhang, J. Zhang, Over 16.5% efficiency in ternary organic solar cells by adding an alloyed acceptor with energy transfer process, Dyes Pigments 192 (2021), 109434.
[21] X. Ma, Y. Mi, F. Zhang, Q. An, M. Zhang, Z. Hu, X. Liu, J. Zhang, W. Tang, Efficient ternary polymer solar cells with two well-compatible donors and one ultranarrow bandgap nonfullerene acceptor, Adv. Energy Mater. 8 (2018), 1702854.

[22] Z. Liu, H. Wang, Ternary polymer solar cells by employing two well-compatible donors with cascade energy levels, Dyes Pigments 192 (2021), 109424.
[23] M. Jiang, H. Bai, H. Zhi, L. Yan, H.Y. Woo, L. Tong, J. Wang, F. Zhang, Q. An, Rational compatibility in a ternary matrix enables all-small-molecule organic solar cells with over 16% efficiency, Energy Environ. Sci. 14 (2021) 3945–3953.
[24] X. Ma, A. Zeng, J. Gao, Z. Hu, C. Xu, J.H. Son, S.Y. Jeong, C. Zhang, M. Li, K. Wang, H. Yan, Z. Ma, Y. Wang, H.Y. Woo, F. Zhang, Approaching 18% efficiency of ternary organic photovoltaics with wide bandgap polymer donor and well compatible Y6:Y6-1O as acceptor, Nat. Sci. Rev. 8 (2021), nwaa305.
[25] Y. Zhang, D. Liu, T.K. Lau, L. Zhan, D. Shen, P.W.K. Fong, C. Yan, S. Zhang, X. Lu, C.S. Lee, J. Hou, H. Chen, G. Li, A novel wide-bandgap polymer with deep ionization potential enables exceeding 16% efficiency in ternary nonfullerene polymer solar cells, Adv. Funct. Mater. 30 (2020), 1910466.
[26] X. Xu, K. Feng, Y.W. Lee, H.Y. Woo, G. Zhang, Q. Peng, Subtle polymer donor and molecular acceptor design enable efficient polymer solar cells with a very small energy loss, Adv. Funct. Mater. 30 (2020), 1907570.
[27] Y. Xie, T. Li, J. Guo, P. Bi, X. Xue, H.S. Ryu, Y. Cai, J. Min, L. Huo, X. Hao, H. Y. Woo, X. Zhan, Y. Sun, Ternary organic solar cells with small nonradiative recombination loss, ACS Energy Lett. 4 (2019) 1196–1203.
[28] L. Xiao, H. Mao, Z. Li, C. Yan, J. Liu, Y. Liu, J.A. Reimer, Y. Min, Y. Liu, Employing a narrow-band-gap mediator in ternary solar cells for enhanced photovoltaic performance, ACS Appl. Mater. Interfaces 12 (2020) 16387–16393.
[29] Y. Tang, J. Yu, H. Sun, Z. Wu, C.W. Koh, X. Wu, B. Liu, J. Wang, Q. Liao, Y. Li, H. Guo, H.Y. Woo, F. Gao, X. Guo, Two compatible polymer donors enabling ternary organic solar cells with a small nonradiative energy loss and broad composition tolerance, Sol. RRL 4 (2020), 2000396.
[30] X. Xu, Z. Bi, W. Ma, G. Zhang, H. Yan, Y. Li, Q. Peng, Stable large area organic solar cells realized by using random terpolymers donors combined with a ternary blend, J. Mater. Chem. A 7 (2019) 14199–14208.
[31] X. Liu, S. Du, Z. Fu, C. Chen, J. Tong, J. Li, N. Zheng, R. Zhang, Y. Xia, Ternary solar cells via ternary polymer donors and third component PC71BM to optimize morphology with 13.15% efficiency, Sol. Energy 222 (2021) 18–26.
[32] Q. An, J. Wang, X. Ma, J. Gao, Z. Hu, B. Liu, H. Sun, X. Guo, X. Zhang, F. Zhang, Two compatible polymer donors contribute synergistically for ternary organic solar cells with 17.53% efficiency, Energy Environ. Sci. 13 (2020) 5039–5047.
[33] D. Dang, D. Yu, E. Wang, Conjugated donor-acceptor terpolymers toward high-efficiency polymer solar cells, Adv. Mater. 31 (2019), 1807019.
[34] W. Su, G. Li, Q. Fan, Q. Zhu, X. Guo, J. Chen, J. Wu, W. Ma, M. Zhang, Y. Li, Nonhalogen solvent-processed polymer solar cells based on chlorine and trialkylsilyl substituted conjugated polymers achieve 12.8% efficiency, J. Mater. Chem. A 7 (2019) 2351–2359.
[35] R. Ma, T. Liu, Z. Luo, Q. Guo, Y. Xiao, Y. Chen, X. Li, S. Luo, X. Lu, M. Zhang, Y. Li, H. Yan, Improving open-circuit voltage by a chlorinated polymer donor endows binary organic solar cells efficiencies over 17%, Sci. China Chem. 63 (2020) 325–330.
[36] B. Huang, L. Chen, X. Jin, D. Chen, Y. An, Q. Xie, Y. Tan, H. Lei, Y. Chen, Alkylsilyl functionalized copolymer donor for annealing-free high performance solar cells with over 11% efficiency: crystallinity induced small driving force, Adv. Funct. Mater. 28 (2018), 1800606.
[37] Y. Cheng, H. Jin, J. Oh, X. Huang, R. Lv, B. Huang, Z. Ma, C. Yang, L. Chen, Y. Chen, Structural similarity induced improvement in the performance of organic solar cells based on novel terpolymer donors, J. Mater. Chem. A 9 (2021) 9238–9247.
[38] Q. An, F. Zhang, J. Zhang, W. Tang, Z. Deng, B. Hu, Versatile ternary organic solar cells: a critical review, Energy Environ. Sci. 9 (2016) 281–322.
[39] W. Su, Q. Fan, X. Guo, X. Meng, Z. Bi, W. Ma, M. Zhang, Y. Li, Two compatible nonfullerene acceptors with similar structures as alloy for efficient ternary polymer solar cells, Nano Energy 38 (2017) 510–517.
[40] D.H. Kaelble, Dispersion-polar surface tension properties of organic solids, J. Adhes. 2 (2008) 66–81.
[41] H. Wang, L. Yang, P.C. Lin, C.C. Chueh, X. Liu, S. Qu, S. Guang, J. Yu, W. Tang, A simple dithieno[3,2-b:2′,3′-d]pyrrol-rhodanine molecular third component enables over 16.7% efficiency and stable organic solar cells, Small 17 (2021), 2007746.
[42] J. Wan, L. Zhang, Q. He, S. Liu, B. Huang, L. Hu, W. Zhou, Y. Chen, High-performance pseudoplanar heterojunction ternary organic solar cells with nonfullerene alloyed acceptor, Adv. Funct. Mater. 30 (2020), 1909760-3575.
[43] Y. Chang, J. Zhang, Y. Chen, G. Chai, X. Xu, L. Yu, R. Ma, H. Yu, T. Liu, P. Liu, Q. Peng, H. Yan, Achieving efficient ternary organic solar cells using structurally similar non-fullerene acceptors with varying flanking side chains, Adv. Energy Mater. 11 (2021), 2100079.
[44] L. Zhan, S. Li, T.-K. Lau, Y. Cui, X. Lu, M. Shi, C.-Z. Li, H. Li, J. Hou, H. Chen, Over 17% efficiency ternary organic solar cells enabled by two non-fullerene acceptors working in an alloy-like model, Energy Environ. Sci. 13 (2020) 635–645.
[45] P.P. Khlyabich, M. Sezen-Edmonds, J.B. Howard, B.C. Thompson, Y.-L. Loo, Formation of organic alloys in ternary-blend solar cells with two acceptors having energy-level offsets exceeding 0.4 eV, ACS Energy Lett. 2 (2017) 2149–2156.
[46] Q. An, J. Zhang, W. Gao, F. Qi, M. Zhang, X. Ma, C. Yang, L. Huo, F. Zhang, Efficient ternary organic solar cells with two compatible non-fullerene materials as one alloyed acceptor, Small 14 (2018), 1802983.
[47] T. Yan, W. Song, J. Huang, R. Peng, L. Huang, Z. Ge, 16.67% rigid and 14.06% flexible organic solar cells enabled by ternary heterojunction strategy, Adv. Mater. 31 (2019), 1902210.
[48] X. Xu, Z. Bi, W. Ma, Z. Wang, W.C.H. Choy, W. Wu, G. Zhang, Y. Li, Q. Peng, Highly efficient ternary-blend polymer solar cells enabled by a nonfullerene acceptor and two polymer donors with a broad composition tolerance, Adv. Mater. 29 (2017), 1704271.
[49] Q. Fan, W. Su, S. Chen, W. Kim, X. Chen, B. Lee, T. Liu, U.A. Méndez-Romero, R. Ma, T. Yang, W. Zhuang, Y. Li, Y. Li, T.-S. Kim, L. Hou, C. Yang, H. Yan, D. Yu, E. Wang, Mechanically robust all-polymer solar cells from narrow band gap acceptors with hetero-bridging atoms, Joule 4 (2020) 658–672.
[50] C. Wang, W. Zhang, X. Meng, J. Bergqvist, X. Liu, Z. Genene, X. Xu, A. Yartsev, O. Inganäs, W. Ma, E. Wang, M. Fahlman, Ternary organic solar cells with minimum voltage losses, Adv. Energy Mater. 7 (2017), 1700390.
[51] Q. Fan, T. Liu, M. Zhang, W. Su, U.A. Méndez-Romero, T. Yang, X. Geng, L. Hou, D. Yu, F. Liu, H. Yan, E. Wang, Weak makes it powerful: the role of cognate small molecules as an alloy donor in 2D/1A ternary fullerene solar cells for finely tuned hierarchical morphology in thick active layers, Small Methods 4 (2020), 1900766.
[52] G.D. Sharma, R. Suthar, A.A. Pestrikova, A.Y. Nikolaev, F.C. Chen, M.L. Keshtov, Efficient ternary polymer solar cells based ternary active layer consisting of conjugated polymers and non-fullerene acceptors with power conversion efficiency approaching near to 15.5%, Sol. Energy 216 (2021) 217–224.
[53] H. Jiang, X. Li, J. Wang, S. Qiao, Y. Zhang, N. Zheng, W. Chen, Y. Li, R. Yang, Ternary polymer solar cells with high efficiency of 14.24% by integrating two well-complementary nonfullerene acceptors, Adv. Funct. Mater. 29 (2019), 1903596.
[54] Z. Hu, L. Yang, W. Gao, J. Gao, C. Xu, X. Zhang, Z. Wang, W. Tang, C. Yang, F. Zhang, Over 15.7% efficiency of ternary organic solar cells by employing two compatible acceptors with similar LUMO levels, Small 16 (2020), 2000441.
[55] L. Yuan, K. Lu, B. Xia, J. Zhang, Z. Wang, Z. Wang, D. Deng, J. Fang, L. Zhu, Z. Wei, Acceptor end-capped oligomeric conjugated molecules with broadened absorption and enhanced extinction coefficients for high-efficiency organic solar cells, Adv. Mater. 28 (2016) 5980–5985.
[56] Y. Wang, D. Qian, Y. Cui, H. Zhang, J. Hou, K. Vandewal, T. Kirchartz, F. Gao, Optical gaps of organic solar cells as a reference for comparing voltage losses, Adv. Energy Mater. 8 (2018), 1801352.
[57] D. Qian, Z. Zheng, H. Yao, W. Tress, T.R. Hopper, S. Chen, S. Li, J. Liu, S. Chen, J. Zhang, X.-K. Liu, B. Gao, L. Ouyang, Y. Jin, G. Pozina, I.A. Buyanova, W.M. Chen, O. Inganäs, V. Coropceanu, J.-L. Bredas, H. Yan, J. Hou, F. Zhang, A.A. Bakulin, F. Gao, Design rules for minimizing voltage losses in high-efficiency organic solar cells, Nat. Mater. 17 (2018) 703–709.
[58] D. Baran, R.S. Ashraf, D.A. Hanifi, M. Abdelsamie, N. Gasparini, J.A. Rohr, S. Holliday, A. Wadsworth, S. Lockett, M. Neophytou, C.J. Emmott, J. Nelson, C. J. Brabec, A. Amassian, A. Salleo, T. Kirchartz, J.R. Durrant, I. McCulloch, Reducing the efficiency–stability–cost gap of organic photovoltaics with highly efficient and stable small molecule acceptor ternary solar cells, Nat. Mater. 16 (2017) 363–369.
[59] B. Fan, W. Zhong, X.-F. Jiang, Q. Yin, L. Ying, F. Huang, Y. Cao, Polymer solar cells: Improved performance of ternary polymer solar cells based on a nonfullerene electron cascade acceptor, Adv. Energy Mater. 7 (2017), 1602127.
[60] W. Zhong, J. Cui, B. Fan, L. Ying, Y. Wang, X. Wang, G. Zhang, X.-F. Jiang, F. Huang, Y. Cao, Enhanced photovoltaic performance of ternary polymer solar cells by incorporation of a narrow-bandgap nonfullerene acceptor, Chem. Mater. 29 (2017) 8177–8186.